C.P. No. 367
(18,998)
A.R.C. Technical Report

C.P. No. 367
(18,998)
A.R.C. Technical Report

MINISTRY OF SUPPLY

AERONAUTICAL RESEARCH COUNCIL

CURRENT PAPERS

Experimental Investigation of the Pressure Distribution at the Centre-Section of a Sweptback Wing at High Subsonic Speeds

By

T. E. B. Bateman, B.A., B.Sc. and A. J. Lawrence, B.Sc.

LONDON: HER MAJESTY'S STATIONERY OFFICE

1957

FIVE SHILLINGS NET

C.P. No. 367

U.D.C. No. 533.691.13.043.2:533.69.048.1

Report No. Aero 2556

August, 1955

ROYAL AIRCRAFT ESTABLISHMENT

Experimental Investigation of the Pressure Distribution at the Centre-section of a Sweptback Wing at High Subsonic Speeds

by

T. E. B. Bateman B.A., B.Sc.
and
A. J. Lawrence B.Sc.

SUMMARY

The uncertainty of the validity of theoretical estimates and the absence of experimental data for the pressure distribution at the centre-section of a sweptback wing at high subsonic speeds led to the present tests. The measurements have been made on a 40° sweptback wing over the Mach number range 0.50 to 0.94, at zero incidence.

Given pressures are reached further aft at the centre-section than on a section of the infinite sheared wing. In particular the supersonic region, when formed, occurs much further aft and the shock-wave moves quickly to a position close behind the trailing edge. The isobars lose their sweep in the neighbourhood of the centre-section and this reduces the critical Mach number from 0.38 for the sheared wing to 0.81 for the centre-section. The maximum local Mach number at the centre-section tends to a steady value of about 1.15 at high subsonic speeds.

Theoretical estimates of the pressure distributions on the sheared wing at zero incidence are shown to agree well with the measured values for speeds at which no shock-waves form but estimates for the centre-section agree well only at very low speeds. At higher speeds (even at M = 0.5) the theory predicts too low a pressure over the forward half of the chord and too low a suction over the rear half, i.e. it underestimates the "centre effect".

LIST OF ILLUSTRATIONS

LIST OF CONTENTS

LIST OF TABLES

LIST OF ILLUSTRATIONS

1 Introduction

The flow at a "kink" or change of sweep of a swept wing can be regarded as that on an infinite sheared wing together with an additional kink effect. One result of the kink effect is that the isobars are brought nearer the edge which is concave when viewed from just outside the wing. On a wing of constant thickness/chord ratio this leads to changes in the local positions of boundary-layer transition and the shock-wave (if any) and in the value of the critical Mach number. Knowledge of the kink effect is required in understanding its influence on the characteristics of an aircraft with a kinked or swept planform. In particular, there is the case of the centre-section of a swept-back wing, where the isobars are unswept. Knowledge of the "centre effect" associated with this is required in designing junction shapes to decrease the drag of wing-body combinations, particularly at transonic speeds.[1,2,3].

Theoretical estimates of the pressure distributions at such central sections (replacing the wing by a system of kinked source-lines) and on infinite sheared wings may be derived for inviscid, incompressible flow[4]. These may be extended to compressible flow according to linear theory (Prandtl-Glauert rule) and with higher order approximations involving the use of the incompressible pressure coefficients in the compressibility factor (Weber rule[5]). In any particular case the difference between the distributions at the centre-section and on the sheared wing shows the magnitude of the "centre effect", although this difference is not given directly by the method of calculation.

Measurements at low speeds have been made on both sheared wings and at the centre-sections of sweptback wings, and agreement with incompressible theory has been good (See for example the comparison for wings of thickness/chord ratio 12% in Ref. 5).

Measurements have also been made at higher speeds of the pressure distributions at several spanwise stations on a sweptback wing, including some at the junction of the wing with a flat-sided body[2]. Certain of these measurements gave a good approximation for the infinite sheared wing, and, regarding the flat-side of the body as a reflection plane, the measurements at this junction were considered to give a good indication of the flow at the equivalent centre-section. However, theoretical estimates did not agree very well with these measurements at high subsonic Mach numbers, and some designs for wing-body junction shape did not produce the desired calculated effects when tested, partly because of this discrepancy.

The need for accurate measurements at high subsonic speeds on an actual centre-section led to the present tests, which have been made on a model used for research on wing-body junction shapes[3]. In the present report, reference to the earlier results[2] is included to enable a comparison to be made between the flow at the centre-section and on the infinite sheared wing, and also to show the accuracy, in both cases, of theoretical estimates according to the Weber rule.

Hereafter, the terms "centre-section" and "centre effect" refer specifically to those of a sweptback wing, and "sheared wing" is used to mean strictly the infinite sheared wing either in the theoretical case or in the experimental approximation (see section 3.3).

2 The Model and Tests

2.1 Details of the Model

The wing used was primarily required, in combination with several different bodies, for tests concerned with the design of junction shapes. It was basically a 40° sweptback wing of symmetrical RAE 101 streamwise section with a thickness/chord ratio of 12%, the maximum thickness being at 31% chord. These values of sweepback and thickness were chosen so that the critical Mach number was well below the choking Mach number of the tunnel, allowing tests to be extended into the supercritical range of Mach number. It was not possible to use either a conventional sting-mounted model or half-model for the centre-section pressure measurements because of the interference of the sting or the tunnel floor in the respective cases. Therefore a complete model of the sweptback wing was designed to be mounted on one tip in the half-model position on the tunnel floor, as shown in Fig. 2. The wing is described in detail in Ref. 3 and leading dimensions are given in Table I.

A floor fairing was designed to cancel any reflection effects from the floor which might have interfered with the flow at the centre-section. Measurements[3], with and without the floor fairing present, showed that it had no noticeable effect on this flow; the centre-section was presumably at a sufficient height above the floor for there to be no interference. The measurements reported here were all made with the floor fairing in position.

Inspection of the model when the tests had been completed, showed that along the centre-section the thickness of the wing varied between 0.005 in. and 0.012 in. oversize (on a chord of 13 in.). Near the trailing edge, however, the presence of the measuring tube increased this to 0.016 in. oversize.

2.2 The Tests

The tests were made in the RAE 10 ft × 7 ft High Speed Wind Tunnel during February 1954. The Reynolds number was 1.3×10^6 based on centre-section chord and the Mach number range was 0.50 to 0.94. The incidence range covered was -1°, 0°, $+1^\circ$ but the tests were primarily concerned with measurements at zero incidence.

Photographs were taken of transition position using the acenaphthene-sublimation technique. Transition was also fixed on one surface of the wing at 10% chord (using a thread of 0.010 in. diameter), and in this condition of the model, the position of the shock-wave was photographed.

Forces measurements, which were made on the wing, both with and without bodies, are reported in Ref. 3.

3 Results

3.1 Preparation

The blockage effect on the free stream Mach number, M_0, was derived by the method of Evans[6] using the force measurements of Ref. 3.

The pressure measurements were recorded as differences between those at the measuring holes on the model and either the working section static pressure or the total head in the settling chamber. These were converted to values of local p/H by the usual procedure for reduction of results. Pressure coefficients, C_p, were computed from these values. Mean values (i.e. of upper and lower surfaces) of p/H and C_p were taken, and the local Mach number M was obtained directly from the mean values of p/H using compressible flow tables*. To obtain the values for the upper and lower surfaces at $+1^{\circ}$, the means were taken between the required surface at $+1^{\circ}$ and the opposite surface at -1°.

The coefficients of the tangential pressure-force, C_T, were obtained by numerical integration of the pressure distribution, as described in Ref. 2. In the present tests at zero incidence, these coefficients are the same as normal-pressure drag coefficients; the term C_T is used for consistency with Ref. 2.

3.2 Accuracy

The blockage effect on M_o varied from 0.001 at M_o = 0.50 to 0.023 at M_o = 0.94, and the corrected value of M_o is expected to be accurate over the whole range of the tests to within ±0.003.

The measurements over the centre section may be in error due to the variations in M_o and of the blockage correction over the model position and to errors in reading the manometers. The maximum errors may reach the following orders:-

	M_o = 0.50	M_o = 0.94
M	±0.003	±0.004
C_p	±0.008	±0.008
p/H	±0.002	±0.003

Small inaccuracies in the incidence at both $\alpha = 0^{\circ}$ and $\pm1^{\circ}$ are overcome by taking the mean values of readings at two surfaces as explained in section 3.1 above. The C_T integrations should be accurate to ±0.0002 (see Ref. 2). The effects of the tip and the floor are considered to be negligible at the centre-section and this assumption is justified by the spanwise variation of the positions of transition and shock-wave shown in Fig. 10 and 11.

3.3 Results from Earlier Tests

Reference is made to two groups of measurements from tests on sting-mounted models described in Refs. 1 and 2. In these tests the wing is fundamentally the same as that of the present tests except for a small difference in the span. Model 2 is a combination of the wing with a flat-sided body. Model 5 is a combination with a body having a modified junction shape and is shown in Fig. 1. The difference in the span, (compare Figs. 1 and 2), is such that the wing outboard of the flat-sided body of Model 2 is exactly the same as the upper part of the present model. Thus the measurements in the wing-body junction of Model 2 correspond directly with those at the present centre-section, and it is now possible to see to what extent measurements in such a junction represent the flow at an actual centre-section. Errors in the junction measurements arise from the holes being in the body rather than the actual junction (about 0.1 in. away, except near the leading edge). There are also boundary-layer interaction effects probably leading to premature separations or the generation of vorticity. The position of transition is well forward in the junction whereas it is towards the rear of the actual centre-section.

* Entropy increase through any shocks being neglected, for the shock strengths present

The wing-body junction shape of Model 5 is designed to give the same flow in the junction as on the infinite sheared wing, at $M_o = 0.87$. Although this is not attained in the junction, the flow at "section f" (see Fig. 1) is seen from measured isobar patterns to give a good approximation for the sheared-wing flow, and better than obtained on any of the other models tested at the same time. Thus "model 5 section f" has been chosen in this report to represent the flow on the infinite sheared wing. At some Mach numbers, the sweepback of some isobars is slightly (2° or 3°) less than 40°.

3.4 Presentation of Results

The mean values of p/H, M (local Mach number) and C_p are tabulated for 0°, and $+1^\circ$ (upper and lower surfaces) in Tables III, IV, V. The values at $+1^\circ$ are for reference only and are not used in this report. The results taken from Ref. 2 (see section 3.3) are the mean values of the upper and lower surface measurements at zero incidence.

Fig. 3 shows the variation with free-stream Mach number of local Mach number, M, over the chord of the sheared wing (i.e. "Model 5 section f"), and Fig. 4 shows that over the centre-section chord. The "three-dimensional" representation of these variations enables certain results to be seen clearly. The local Mach number is plotted in preference to the pressure coefficient as it shows more clearly the growth of the supersonic region and associated differences between the centre section and sheared wing. In order to spread out the curves at high free-stream Mach numbers, a logarithmic scale of $(1-M_o^2)^{\frac{1}{2}}$ is used. Also, to illustrate the important trends, the locus of the positions of maximum local Mach number M_{max} and the contour of $M = 1.00$ are shown as thick lines. Contours are drawn for several other local Mach numbers and thin lines give a guide to the chordwise position over the figures. It should be noted that the individual distributions are frequently at different values of M_o for the two sections tested.

Figures of experimental (interpolated where required) and theoretical pressure distributions are shown for $M_o = 0.50$, 0.82, 0.86 and 0.90 (Fig. 5 a, b, c, d). These four Mach numbers are considered sufficient to compare the effects of compressibility on the flow at the two sections, and the manner in which the theory fails. The centre effect is shown in Fig. 6 at three Mach numbers for both the theoretical and experimental cases. It is obtained directly from the values used in plotting Fig. 5 as the difference between the pressure coefficients at the centre-section and those at corresponding positions on the sheared wing.

The variations of trailing-edge pressure coefficients, maximum local Mach number, and tangential pressure-force coefficient are of interest at the higher Mach numbers and are plotted against the free-stream Mach number in Figs. 7, 8 and 9. The earlier measurements of C_T at different spanwise positions were found in Ref. 2 to fit straight line approximations when plotted against $(1-M^2)^{\frac{1}{2}}$. Similar approximations do not fit very closely with results for the centre section, which are therefore shown plotted against M_o only.

Photographs of the positions of transition and shock-wave are shown in Figs. 10 and 11.

4 Discussion of Results

4.1 Variation of Local Mach Number

On the infinite sheared wing the isobars are swept at 40°, and since the streamline, in plan view, is curved, the measured local Mach number at any point is the maximum at that point rather than the streamwise component. On the other hand, the symmetry of the centre-section means that the isobars there are unswept and the velocities at the centre section are everywhere in a streamwise direction. Thus the measured Mach number at any point on the centre section is the maximum at the point and is also normal to the isobars.

The critical Mach number, M_{crit}, is here defined as that at which the component of the local Mach number normal to the isobars first reaches unity.

4.1.1 The Sheared Wing (Ref. 2)

The position on the chord of the maximum local Mach number, M_{max}, is seen from Fig. 3 to move only slightly rearwards along the chord with increasing free-stream Mach number. A local Mach number of unity is first reached at about $M_o = 0.80$. The supersonic region, enclosed by the heavy contour of $M = 1.00$ gradually expands with increasing Mach number, extending principally over the forward half of the chord.

The critical Mach number as defined above (section 4.1) occurs at about $M_o = M_{crit} = 0.88$. This has been obtained using a calculated deviation of the streamline from the free-stream direction of about 7° in the region of 30% chord. Estimation according to the Weber rule also gives $M_{crit} = 0.88$.

The shock-wave is not as clearly defined on the Mach number distributions as on the distributions of pressure coefficient. However, there are kinks in the contours of constant local Mach number which are probably associated with the formation of the shock-wave. In particular the contour for $M = 1.10$ has a distinct kink where it crosses the distribution for $M_o = 0.894$; this suggests that the shock-wave forms at about this free-stream Mach number, although it is not strong enough to show on the distribution of local Mach number. The maximum local Mach number is then 1.24 and its component normal to the isobars is approximately 1.05.

4.1.2 The Centre-Section

Comparison of Figs. 3 and 4 shows primarily the general characteristic of the centre-section, viz. that the isobars, maximum local Mach numbers (peak suctions) and associated effects occur further aft than on the section of the sheared wing. The supersonic region enclosed by the line $M = 1.00$ lies at the rear of the section instead of being mostly in the forward half. From Fig. 10 it is seen that transition at the centre section occurs at about 0.85c at $M_o = 0.5$ and at almost 1.0c at $M_o = 0.91$, whereas the corresponding positions for the sheared wing[1] are 0.45c and 0.57c. Also from Fig. 10 an idea may be obtained of the spanwise extent of the centre effect.

At the centre-section the critical Mach number, as defined above (section 4.1), occurs at $M_o = M_{crit} = 0.81$. This is the same value as a theoretical estimate according to the Weber rule.

The rearward movement of the position of the maximum local Mach number with increasing free-stream Mach number is much more marked than on the sheared wing, although at $M_o = 0.5$ the position at the centre-section is only about 0.1 chord aft of that on the sheared wing. In particular it moves back rapidly in the range $M_o = 0.84$ to 0.88, probably as a result of the development of a shockwave. Although the shock-wave is not strong enough to be distinguished on any particular distribution of local Mach number (or of C_p) in this region, the first sign of it is assumed to be the increased movement in the position of M_{max} at about $M_o = 0.84$. At this Mach number the value of M_{max} is 1.05, which is the same value as the component of M_{max} normal to the isobars on the sheared wing when the shock-wave first appears there (section 4.1.1). Thus the shock-wave appears to form at about 70% chord (where M = 1) at M_o = 0.84 and it moves rapidly back to the trailing edge by M_o = 0.89 (see also section 4.3). The photographs showing the shock-wave position (the dark lines on Fig. 11) confirm that it is at the trailing edge of the centre-section at M_o = 0.91. There is a suggestion of a bifurcated shock-wave pattern occurring over the mid-span portion of the wing but there is no sign of the weak forward limb on any of the centre-section measurements and it is presumed to have died out at this section.

4.2 Pressure Distributions

4.2.1 The Sheared Wing (Ref. 2)

The theoretical estimates (calculated on the principles of Refs. 4 and 5) are seen (Fig. 5) to agree well with the experimental curves at Mach numbers up to M_o = 0.86. The very good agreement over the first 30% chord at M = 0.82 and 0.86 is rather fortuitous. The agreement in this region at M_o = 0.5 is not as good and the consistent discrepancy here cannot be completely explained by the possible error in C_p of ±0.008.

The theoretical distributions have been calculated for $\phi = 40^o$. The possible effect of the actual isobar sweep differing slightly from 40^o (see end of section 3.3) is indicated by theoretical calculations for different values of ϕ. For example, at M_o = 0.86 and x/c = 0.309 (near the position of peak suction) the theoretical pressure coefficient for $\phi = 35^o$ is -0.581, whereas for $\phi = 40^o$ it is -0.487 as in Fig. 5(c). Thus the theoretical distributions, and presumably the experimental ones too, are sensitive to deviations from the nominal angle of sweep. The fact that some of the isobars are slightly less swept than 40^o on "Model 5 section f" means that on the truly infinite sheared wing the suctions might be rather less than the measured ones in Fig. 5. In general the agreement between theory and experiment is very satisfactory at subcritical Mach numbers. It should be noted that the steep pressure rises on the experimental curves of M_o = 0.82 and 0.86 (in particular) do not represent shock-waves since M_{crit} = 0.88.*

4.2.2 The Centre-Section

The distributions in Fig. 5 include those measured in the junction of the wing with a flat-sided body (see section 3.3). Although these measurements agree in a general way with the present centre-section measurements, they indicate that if accurate measurements are required for the centre-sections of swept wings it is necessary to make the measurements at the actual centre-section.

The theoretical distribution has been shown to agree well with experiment in the incompressible flow case[5] and the agreement is still good at M_o = 0.50 (Fig. 5). At M_o = 0.82, however, a serious discrepancy with the actual distribution is seen to have arisen. The magnitude of the peak suction C_p is reasonably correct, (thus the estimated value of M_{crit} agrees with experiment) but its calculated rearward movement due to the centre effect is considerably less than actually occurs.

The Weber rule does not strictly apply at supercritical Mach numbers, but there are no sudden changes at the critical Mach number (M_o = 0.81) in the theoretical distributions so that the comparisons at M = 0.82 and 0.86

---

* An interesting point is illustrated in Fig. 5(d) which shows the differences between the pressure distributions when a shock-wave is present and when it is not. Provided flow separation does not occur, the distribution behind the shock-wave is nearly the same as that without the shock-wave.

merely accentuate the discrepancies at high subcritical speeds. The compressibility factor becomes indeterminate over part of the chord by $M_o = 0.90$ and no theoretical distribution for the centre-section is shown on Fig. 5(d).

4.2.3 The Centre Effect

The centre effect itself is derived as the difference between the pressure distributions at the centre and on the sheared wing. The comparison between the centre effects derived from theory and experiment is shown in Fig. 6. This indicates the type of error to be allowed for if similar calculations are made in such cases as wing-body junction design, when the important consideration is the centre effect itself. At the lower speeds the theoretical estimate is satisfactory, but the approximations in deriving the compressibility effects cause poorer estimates at higher speeds. The correction to the theory as it now stands requires, in general, an increase in pressure over the forward half of the chord, and a decrease over the rear, i.e. the centre effect is at present underestimated.

4.3 Trailing-Edge Pressure

The variation of the trailing-edge pressure coefficient with free-stream Mach number M_o is shown in Fig. 7.

It has been found that the variation of this coefficient gives a good indication of flow separation, by showing an increase in trailing edge suction (e.g. Ref. 7, Fig. 27). Such an increase also occurs if the shock-wave on the wing moves back to, or behind, the trailing edge before separation occurs. The pressure distributions show that no separations were present in these tests; in the case of the sheared wing, insufficiently high Mach numbers were reached and at the centre-section the shock-wave moved quickly back to, or behind the trailing edge. Thus the changes in trailing edge pressure shown in Fig. 7 illustrate only the development and movement of the shock-waves on the two sections.

At both the centre-section and on the sheared wing there is seen to be a slight increase in pressure above the free-stream Mach numbers at which the shock-wave is assumed to begin developing (i.e. $M_o = 0.84$ and 0.894 respectively, see section 4.2.1). The most significant result is the sudden rise in suction when the shock-wave moves back to the trailing edge at the centre section at about $M_o = 0.89$. This gives the clearest indication of the Mach number at which the shock-wave reaches the trailing edge. The increased suction above $M_o = 0.89$ shows that the shock-wave is downstream of the measuring hole, so that it would appear that the shock-wave is slightly detached upstream from the trailing edge through boundary-layer interaction.

4.4 Maximum Local Mach Number

The chordwise movement of maximum local Mach number, M_{max}, can be seen in Figs. 3 and 4 and has been discussed in sections 4.1.1 and 4.2.1. The variation of the magnitude of M_{max} with free-stream Mach number, M_o, is shown in Fig. 8.

At the centre-section the rate of increase of M_{max} with M_o falls off at the highest Mach numbers tested and tends to zero at about $M_{max} = 1.15$. As is seen from Fig. 4 the chordwise Mach number distributions become quite flat so that a value close to the maximum is maintained over an appreciable chordwise distance.

On the sheared wing the increase of M_{max} continues as far as the tests were made, i.e. up to $M_0 = 0.91$ but other tests (Ref. 7) have shown that this rate of increase dies away and, at higher subsonic Mach numbers, M_{max} levels off in the region 1.3 to 1.5. It is consistent with the effects of sweepback that this effect on M_{max} occurs at higher free-stream Mach numbers on the sheared wing and that the peak value itself is higher than at the centre-section.

It is clear that no sudden changes in the magnitude of M_{max} occur during formation of the shock-wave at either of the sections tested, not even in the region of rapid movement of the shock-wave at the centre-section between $M = 0.84$ and 0.89.

4.5 Tangential Pressure-Force Coefficient

The variations of the tangential pressure-force coefficient, C_T, with free-stream Mach number M_0 for both the centre-section and sheared wing are shown in Fig. 9.

In general the high values of C_T at the centre-section are due to the positions of the isobars and peak suction being further aft than on the sheared wing. The rapid increase of C_T with M_0 is partly due to the continual rearward movement of the peak suction and partly due to the general increase of suction. When the shock-wave develops it is unswept and therefore stronger at the centre-section and the associated drag is higher.

At the centre-section the values of C_T falls off at the highest Mach numbers ($M_0 > 0.91$). This is principally due to the fall off in the rate of increase of M_{max} (see section 4.4) and the fact that the shock-wave so quickly establishes itself at the trailing edge that the usual continued drag increase due to the shock-wave moving aft cannot occur.

5 Conclusions

Measurements have been made of the pressure distributions at the centre of a sweptback wing at zero incidence for Mach numbers between 0.5 and 0.94. These were required to extend earlier work at low speeds and for comparison with theoretical estimates.

The principal difference between the pressure distribution at the centre-section of a sweptback wing and that on an infinite sheared wing (of the same sweep) is that the pressures are increased over the front part of the centre-section and reduced over the rear part. This difference, which is clearly seen in the measurements, occurs at all subsonic Mach numbers, becoming more pronounced as the free-stream Mach number M_0 is raised. As a result, transition, the peak suction, the shock-wave and the supersonic region all occur nearer the trailing edge of the centre-section than on the infinite sheared wing.

It follows that a loss of sweep of the isobars occurs in the neighbourhood of the centre-section. This reduces the critical Mach number (when the component of local Mach number normal to the isobars reaches unity) from $M_0 = 0.88$ for the sheared wing (taken from Ref. 2) to $M_0 = 0.81$ for the centre-section. Various results for both sections indicate that the shock-wave begins to form when the component of local Mach number normal to the isobars is about 1.05, i.e. $M_0 = 0.894$ for the sheared wing and 0.84 at the centre-section. At higher Mach numbers, whereas on the sheared wing the shock-wave moves only slowly rearwards over the chord and the supersonic region is largely ahead of 50% chord, on the centre-section the shock-wave moves rapidly to the trailing edge, where its arrival at

$M_o = 0.89$ is shown up very clearly by a sudden increase in trailing edge suction. The supersonic region is then largely over the rear half of the chord.

At the centre-section the increase of M_{max} with M_o gradually falls off above about $M_o = 0.90$ so that M_{max} tends to a value of about 1.15. This is expected to occur on the sheared wing at higher values of M_o and to tend to a higher value of M_{max}, nearer 1.5.

The values of tangential pressure-force coefficient, C_T, are much higher at the centre-section than on the sheared wing, and because of the continuous rearward movement of the supersonic region, they increase rapidly with increasing M_o. However when the increase of M_{max} falls off and the shock-wave is well established at the trailing edge the value of C_T actually decreases slightly, i.e. above $M_o = 0.90$.

The theoretical pressure distributions on the sheared wing and at the centre-section agree well with the measured values at low speeds and the allowance for compressibility according to the Weber rule gives good agreement with the sheared wing measurements up to about $M_o = 0.86$ (just below the critical). At the centre-section however, the agreement is not so good at high speeds, principally because the estimated rearward movement of the position of peak suction is too small. In general at the centre-section the theory gives too low a pressure over the forward half of the chord and too low a suction over the rear half, i.e. insufficient allowance is made for the "centre effect". The theoretical values of critical Mach numbers on both the sheared wing and centre-section agree well with experiment.

Previous measurements in the junction of the wing with a flat-sided body give only a fair indication of the pressure distribution at the actual centre-section, the error involved being of the order of 0.1 in C_p.

LIST OF SYMBOLS

x	distance downstream from leading edge of section
c	wing chord (except near tips)
α	nominal incidence
M	local Mach number
M_{max}	maximum local Mach number
M_o	free-stream Mach number
p	local static pressure
H	free-stream total head
C_p	pressure coefficient
C_T	tangential pressure-force coefficient, made non-dimensional by free stream dynamic pressure and wing chord.

REFERENCES

No.	Author	Title, etc.
1	D. E. Hartley	Investigation at high subsonic speeds of wing-fuselage intersection shapes for swept-back wings. Part I. Force measurements on some initial designs. RAE Report No. Aero 2464, May 1952 ARC 15165.
2	D. E. Hartley	Investigation at high subsonic speeds of wing-fuselage intersection shapes for swept-back wings. Part II. Pressure measurements on some initial designs. RAE Report No. Aero 2503, Dec. 1953 ARC 16780.
3	T. E. B. Bateman D. J. Harper	Further tests at high subsonic speeds in the RAE 10 ft x 7 ft Wind Tunnel on wing-fuselage intersection shapes for sweptback wings. (Unpublished R.A.E. Report).
4	J. Weber	The calculation of the pressure distribution over the surface of two-dimensional and swept wings with symmetrical aerofoil sections. R & M 2918, July 1953.
5	D. Küchemann J. Weber	The subsonic flow past swept wings at zero lift without and with body. R & M 2908, March 1953.
6	J. Y. G. Evans	Corrections to velocity for wall constraint in any 10 x 7 rectangular subsonic wind tunnel. R & M 2662, April 1949.
7	D. W. Holder H. H. Pearcey G. E. Gadd	The interaction between shock waves and boundary layers. C.P. 180, Feb. 1954.

TABLE I

Leading Dimensions of Wing

Sweepback	40°
Chord (except near tips)	13 in.
Mean chord	12.66 in.
Span	43.4 in.
Area	3.82 sq ft
Aspect Ratio	3.43
Section: Symmetrical RAE 101	(max. thickness at 0.31C)
Thickness-chord ratio	0.12

TABLE II

Positions of Pressure Points (at symmetrical positions on upper and lower surfaces)

x/c	Inches aft of Leading Edge
0	0
0.0025	0.033
0.01	0.130
0.03	0.390
0.05	0.650
0.08	1.040
0.13	1.690
0.20	2.600
0.30	3.900
0.40	5.200
0.50	6.500
0.60	7.800
0.70	9.100
0.80	10.400
0.90	11.700
1.00	13.000

TABLE III

Values of $^{P}/_{H}$

α	$M_o \approx 0.50$ 0°	$M_o \approx 0.50$ +1° Upper Surface	$M_o \approx 0.50$ +1° Lower Surface	$M_o \approx 0.75$ 0°	$M_o \approx 0.75$ +1° Upper Surface	$M_o \approx 0.75$ +1° Lower Surface	$M_o \approx 0.82$ 0°	$M_o \approx 0.82$ +1° Upper Surface	$M_o \approx 0.82$ +1° Lower Surface	α
$100\ ^{x}/_{c}$ \\ M_o	0.501	0.500	0.500	0.750	0.752	0.752	0.820	0.819	0.819	M_o / $100\ ^{x}/_{c}$
00	1.000	1.000	1.000	0.999	0.999	0.999	1.000	0.999	0.999	00
0.25	0.964	0.956	0.971	0.934	0.921	0.944	0.927	0.915	0.938	0.25
01	0.920	0.910	0.929	0.855	0.840	0.869	0.838	0.826	0.855	01
03	0.875	0.865	0.885	0.772	0.756	0.786	0.748	0.733	0.763	03
05	0.856	0.847	0.866	0.736	0.720	0.750	0.708	0.693	0.723	05
08	0.840	0.832	0.850	0.702	0.686	0.716	0.669	0.654	0.684	08
13	0.828	0.820	0.837	0.674	0.659	0.688	0.637	0.623	0.652	13
20	0.814	0.807	0.822	0.643	0.627	0.655	0.600	0.586	0.614	20
30	0.800	0.793	0.808	0.606	0.589	0.618	0.553	0.538	0.572	30
40	0.797	0.792	0.804	0.590	0.573	0.603	0.525	0.509	0.543	40
50	0.802	0.797	0.808	0.595	0.578	0.606	0.522	0.503	0.540	50
60	0.808	0.805	0.814	0.607	0.592	0.616	0.532	0.513	0.549	60
70	0.817	0.814	0.821	0.624	0.617	0.627	0.551	0.534	0.567	70
80	0.827	0.824	0.829	0.646	0.642	0.647	0.580	0.570	0.586	80
90	0.837	0.836	0.838	0.671	0.668	0.670	0.618	0.619	0.621	90
100	0.857	0.857	0.857	0.716	0.714	0.714	0.673	0.675	0.675	100

TABLE III (Cont.)

Values of P/H

	$M_o \approx 0.84$			$M_o \approx 0.86$			$M_o \approx 0.88$			
α	0^{o}	$+1^{o}$ Upper Surface	$+1^{o}$ Lower Surface	0^{o}	$+1^{o}$ Upper Surface	$+1^{o}$ Lower Surface	0^{o}	$+1^{o}$ Upper Surface	$+1^{o}$ Lower Surface	α
$100\ x/c$ \ M_o	0.840	0.840	0.840	0.861	0.861	0.861	0.881	0.880	0.880	M_o / $100\ x/c$
00	0.999	0.999	0.999	0.999	0.999	0.999	1.000	0.999	0.999	00
0.25	0.925	0.913	0.936	0.924	0.912	0.935	0.923	0.912	0.934	0.25
01	0.836	0.822	0.852	0.833	0.820	0.849	0.831	0.816	0.844	01
03	0.741	0.727	0.757	0.736	0.723	0.753	0.732	0.717	0.746	03
05	0.700	0.686	0.716	0.694	0.681	0.710	0.688	0.674	0.703	05
08	0.660	0.646	0.676	0.652	0.639	0.669	0.646	0.631	0.660	08
13	0.627	0.613	0.642	0.617	0.605	0.633	0.610	0.596	0.624	13
20	0.588	0.575	0.604	0.578	0.566	0.594	0.570	0.557	0.584	20
30	0.540	0.526	0.555	0.527	0.515	0.544	0.519	0.506	0.533	30
40	0.508	0.492	0.526	0.492	0.479	0.509	0.482	0.469	0.497	40
50	0.499	0.481	0.519	0.479	0.465	0.498	0.467	0.453	0.483	50
60	0.507	0.481	0.527	0.475	0.460	0.502	0.461	0.446	0.477	60
70	0.524	0.500	0.544	0.487	0.463	0.519	0.462	0.447	0.486	70
80	0.552	0.532	0.567	0.512	0.482	0.541	0.476	0.454	0.507	80
90	0.601	0.607	0.603	0.560	0.515	0.579	0.503	0.480	0.538	90
100	0.662	0.663	0.663	0.652	0.656	0.656	0.647	0.601	0.601	100

TABLE III (Cont.)

Values of $^{p}/_{H}$

α	$M_o \approx 0.89$ 0°	$M_o \approx 0.89$ +1° Upper Surface	$M_o \approx 0.89$ +1° Lower Surface	$M_o \approx 0.90$ 0°	$M_o \approx 0.90$ +1° Upper Surface	$M_o \approx 0.90$ +1° Lower Surface	$M_o \approx 0.91$ 0°	$M_o \approx 0.91$ +1° Upper Surface	$M_o \approx 0.91$ +1° Lower Surface	α
100 $^{x}/_{c}$ \ M_o	0.891	0.891	0.891	0.902	0.902	0.902	0.912	0.913	0.913	M_o / 100 $^{x}/_{c}$
00	1.000	0.999	0.999	0.999	0.999	0.999	1.000	0.999	0.999	00
0.25	0.923	0.911	0.931	0.922	0.942	0.933	0.924	0.911	0.932	0.25
01	0.830	0.812	0.841	0.829	0.817	0.844	0.828	0.814	0.841	01
03	0.730	0.712	0.741	0.728	0.717	0.745	0.727	0.713	0.740	03
05	0.686	0.669	0.697	0.684	0.673	0.700	0.682	0.668	0.695	05
08	0.643	0.626	0.654	0.641	0.629	0.657	0.638	0.625	0.652	08
13	0.607	0.590	0.618	0.604	0.594	0.620	0.602	0.589	0.615	13
20	0.567	0.551	0.577	0.564	0.553	0.579	0.561	0.548	0.573	20
30	0.515	0.500	0.526	0.511	0.502	0.526	0.508	0.497	0.523	30
40	0.478	0.462	0.488	0.473	0.463	0.488	0.470	0.458	0.482	40
50	0.462	0.445	0.473	0.456	0.446	0.473	0.452	0.441	0.465	50
60	0.455	0.434	0.467	0.449	0.438	0.465	0.444	0.432	0.457	60
70	0.455	0.438	0.469	0.448	0.438	0.465	0.443	0.431	0.456	70
80	0.463	0.445	0.480	0.452	0.441	0.469	0.445	0.433	0.459	80
90	0.486	0.467	0.502	0.468	0.459	0.484	0.453	0.445	0.465	90
100	0.571	0.552	0.552	0.492	0.485	0.485	0.476	0.471	0.471	100

TABLE III (Cont.)

Values of $^P/H$

$M_o \approx 0.925$				$M_o \approx 0.94$			
α	0^o	$+1^o$ Upper Surface	$+1^o$ Lower Surface	0^o	$+1^o$ Upper Surface	$+1^o$ Lower Surface	α
M_o / 100 $^x/_c$	0.926	0.925	0.925	0.940	0.940	0.940	M_o / 100 $^x/_c$
00	1.000	0.999	0.999	1.000	0.999	0.999	00
0.25	0.923	0.910	0.931	0.921	0.910	0.931	0.25
01	0.826	0.813	0.839	0.826	0.812	0.839	01
03	0.724	0.711	0.739	0.724	0.710	0.737	03
05	0.680	0.666	0.694	0.679	0.665	0.692	05
08	0.636	0.623	0.650	0.634	0.621	0.648	08
13	0.599	0.587	0.612	0.597	0.584	0.610	13
20	0.557	0.546	0.570	0.555	0.543	0.568	20
30	0.505	0.494	0.517	0.502	0.491	0.515	30
40	0.466	0.455	0.478	0.463	0.452	0.475	40
50	0.448	0.437	0.462	0.445	0.433	0.458	50
60	0.440	0.428	0.453	0.436	0.424	0.449	60
70	0.438	0.427	0.452	0.434	0.422	0.447	70
80	0.439	0.428	0.454	0.435	0.424	0.448	80
90	0.444	0.435	0.456	0.438	0.428	0.450	90
100	0.467	0.463	0.463	0.461	0.456	0.456	100

TABLE IV

Values of M

α	$M_o \approx 0.50$			$M_o \approx 0.75$			$M_o \approx 0.82$			α
	0^o	$+1^o$		0^o	$+1^o$		0^o	$+1^o$		
		Upper Surface	Lower Surface		Upper Surface	Lower Surface		Upper Surface	Lower Surface	
M_o / 100 x/c	0.501	0.500	0.500	0.750	0.752	0.752	0.820	0.819	0.819	M_o / 100 x/c
00	0	0.022	0.022	0.043	0.043	0.043	0.027	0.042	0.042	00
0.25	0.231	0.256	0.206	0.315	0.345	0.288	0.332	0.358	0.304	0.25
01	0.348	0.371	0.327	0.478	0.506	0.453	0.509	0.529	0.478	01
03	0.441	0.460	0.421	0.620	0.646	0.597	0.658	0.681	0.634	03
05	0.475	0.493	0.457	0.677	0.702	0.654	0.720	0.743	0.697	05
08	0.504	0.520	0.487	0.729	0.754	0.707	0.780	0.803	0.757	08
13	0.526	0.539	0.511	0.772	0.796	0.751	0.829	0.851	0.807	13
20	0.550	0.563	0.536	0.820	0.845	0.801	0.887	0.908	0.864	20
30	0.574	0.585	0.561	0.878	0.904	0.858	0.960	0.984	0.930	30
40	0.578	0.588	0.567	0.902	0.929	0.882	1.005	1.032	0.976	40
50	0.571	0.579	0.561	0.894	0.920	0.878	1.011	1.041	0.980	50
60	0.560	0.566	0.551	0.876	0.899	0.861	0.994	1.025	0.967	60
70	0.545	0.550	0.539	0.850	0.860	0.845	0.964	0.991	0.938	70
80	0.528	0.533	0.524	0.816	0.822	0.813	0.918	0.934	0.908	80
90	0.510	0.512	0.509	0.777	0.782	0.778	0.858	0.857	0.854	90
100	0.475	0.475	0.475	0.708	0.711	0.711	0.775	0.771	0.771	100

TABLE IV (Cont.)

Values of M

α	$M_o \approx 0.84$ 0°	$M_o \approx 0.84$ +1° Upper Surface	$M_o \approx 0.84$ +1° Lower Surface	$M_o \approx 0.86$ 0°	$M_o \approx 0.86$ +1° Upper Surface	$M_o \approx 0.86$ +1° Lower Surface	$M_o \approx 0.88$ 0°	$M_o \approx 0.88$ +1° Upper Surface	$M_o \approx 0.88$ +1° Lower Surface	α
M_o / 100 x/c	0.840	0.840	0.840	0.861	0.861	0.861	0.881	0.880	0.880	M_o / 100 x/c
00	0.041	0.041	0.041	0.041	0.041	0.041	0.027	0.034	0.034	00
0.25	0.335	0.362	0.308	0.339	0.365	0.312	0.339	0.366	0.314	0.25
01	0.512	0.536	0.484	0.518	0.541	0.490	0.522	0.547	0.498	01
03	0.669	0.691	0.643	0.676	0.697	0.650	0.683	0.706	0.660	03
05	0.732	0.754	0.708	0.742	0.762	0.717	0.750	0.773	0.728	05
08	0.794	0.816	0.769	0.806	0.826	0.780	0.816	0.839	0.794	08
13	0.845	0.866	0.822	0.859	0.879	0.835	0.870	0.892	0.841	13
20	0.904	0.926	0.881	0.921	0.940	0.896	0.933	0.954	0.911	20
30	0.982	1.004	0.957	1.001	1.021	0.975	1.015	1.036	0.993	30
40	1.034	1.059	1.005	1.059	1.082	1.031	1.077	1.099	1.051	40
50	1.049	1.079	1.014	1.083	1.106	1.051	1.102	1.126	1.076	50
60	1.034	1.079	1.002	1.088	1.115	1.044	1.113	1.139	1.085	60
70	1.007	1.046	0.975	1.068	1.109	1.015	1.110	1.138	1.070	70
80	0.961	0.995	0.938	1.027	1.076	0.979	1.088	1.124	1.035	80
90	0.884	0.875	0.881	0.949	1.022	0.919	1.041	1.080	0.985	90
100	0.791	0.789	0.789	0.805	0.800	0.800	0.813	0.885	0.885	100

TABLE IV (Cont.)

Values of M

α	$M_o \approx 0.89$ 0°	$M_o \approx 0.89$ +1° Upper Surface	$M_o \approx 0.89$ +1° Lower Surface	$M_o \approx 0.90$ 0°	$M_o \approx 0.90$ +1° Upper Surface	$M_o \approx 0.90$ +1° Lower Surface	$M_o \approx 0.91$ 0°	$M_o \approx 0.91$ +1° Upper Surface	$M_o \approx 0.91$ +1° Lower Surface	α
$100\ ^x/_c$ \ M_o	0.891	0.891	0.891	0.902	0.902	0.902	0.912	0.913	0.913	M_o / $100\ ^x/_c$
00	0.027	0.043	0.043	0.041	0.023	0.023	0	0.044	0.044	00
0.25	0.341	0.366	0.322	0.343	0.292	0.317	0.339	0.367	0.319	0.25
01	0.524	0.553	0.504	0.525	0.544	0.497	0.527	0.550	0.505	01
03	0.686	0.713	0.668	0.689	0.706	0.662	0.691	0.713	0.669	03
05	0.754	0.780	0.736	0.757	0.774	0.732	0.760	0.782	0.740	05
08	0.820	0.846	0.802	0.824	0.842	0.798	0.827	0.848	0.806	08
13	0.875	0.901	0.859	0.880	0.895	0.855	0.884	0.904	0.864	13
20	0.939	0.964	0.922	0.944	0.960	0.919	0.948	0.967	0.929	20
30	1.021	1.047	1.005	1.028	1.043	1.003	1.033	1.051	1.009	30
40	1.084	1.111	1.067	1.092	1.109	1.067	1.098	1.117	1.077	40
50	1.112	1.141	1.091	1.121	1.138	1.092	1.128	1.148	1.105	50
60	1.124	1.160	1.102	1.134	1.153	1.106	1.142	1.164	1.119	60
70	1.122	1.154	1.100	1.136	1.152	1.106	1.144	1.166	1.121	70
80	1.109	1.141	1.079	1.129	1.148	1.099	1.141	1.162	1.117	80
90	1.070	1.102	1.043	1.101	1.116	1.073	1.126	1.142	1.106	90
100	0.932	0.962	0.962	1.061	1.072	1.072	1.086	1.095	1.095	100

TABLE IV (Cont.)

Values of M

α	$M_o \approx 0.925$ 0°	$M_o \approx 0.925$ +1° Upper Surface	$M_o \approx 0.925$ +1° Lower Surface	$M_o \approx 0.94$ 0°	$M_o \approx 0.94$ +1° Upper Surface	$M_o \approx 0.94$ +1° Lower Surface	α
M_o / 100 x/c	0.926	0.925	0.925	0.940	0.940	0.940	M_o / 100 x/c
00	0.027	0.011	0.011	0.027	0.026	0.026	00
0.25	0.341	0.369	0.320	0.346	0.370	0.321	0.25
01	0.529	0.553	0.506	0.530	0.553	0.508	01
03	0.695	0.715	0.672	0.696	0.717	0.675	03
05	0.764	0.785	0.743	0.765	0.786	0.745	05
08	0.831	0.851	0.810	0.834	0.855	0.813	08
13	0.888	0.907	0.868	0.891	0.911	0.871	13
20	0.953	0.971	0.933	0.956	0.976	0.937	20
30	1.039	1.057	1.018	1.042	1.062	1.022	30
40	1.105	1.123	1.083	1.109	1.128	1.089	40
50	1.136	1.155	1.112	1.141	1.161	1.119	50
60	1.150	1.172	1.126	1.157	1.180	1.134	60
70	1.153	1.173	1.128	1.160	1.182	1.136	70
80	1.151	1.171	1.125	1.158	1.180	1.135	80
90	1.143	1.159	1.121	1.153	1.171	1.132	90
100	1.102	1.110	1.110	1.113	1.121	1.121	100

TABLE V

Values of C_p

α	$M_o \approx 0.50$ 0°	$M_o \approx 0.50$ +1° Upper Surface	$M_o \approx 0.50$ +1° Lower Surface	$M_o \approx 0.75$ 0°	$M_o \approx 0.75$ +1° Upper Surface	$M_o \approx 0.75$ +1° Lower Surface	$M_o \approx 0.82$ 0°	$M_o \approx 0.82$ +1° Upper Surface	$M_o \approx 0.82$ +1° Lower Surface	α
$100\ ^x/_c$ \ M_o	0.501	0.500	0.500	0.750	0.752	0.752	0.820	0.819	0.819	M_o \ $100\ ^x/_c$
00	+1.065	+1.061	+1.061	+1.144	+1.145	+1.145	+1.178	+1.175	+1.175	00
0.25	+0.818	+0.763	+0.866	+0.904	+0.859	+0.944	+0.937	+0.898	+0.974	0.25
01	+0.521	+0.451	+0.582	+0.615	+0.560	+0.667	+0.643	+0.604	+0.700	01
03	+0.221	+0.152	+0.286	+0.306	+0.251	+0.363	+0.346	+0.296	+0.395	03
05	+0.096	+0.030	+0.160	+0.174	+0.119	+0.232	+0.214	+0.164	+0.261	05
08	-0.014	-0.076	+0.049	+0.050	-0.006	+0.106	+0.085	+0.035	+0.134	08
13	-0.097	-0.152	-0.040	-0.052	-0.105	+0.002	-0.020	-0.069	+0.026	13
20	-0.190	-0.244	-0.139	-0.168	-0.223	-0.117	-0.143	-0.191	-0.097	20
30	-0.287	-0.336	-0.238	-0.306	-0.362	-0.254	-0.298	-0.349	-0.238	30
40	-0.306	-0.346	-0.263	-0.364	-0.422	-0.311	-0.389	-0.447	-0.334	40
50	-0.275	-0.309	-0.236	-0.346	-0.400	-0.300	-0.401	-0.465	-0.342	50
60	-0.231	-0.258	-0.198	-0.301	-0.350	-0.260	-0.367	-0.432	-0.314	60
70	-0.173	-0.192	-0.150	-0.240	-0.258	-0.223	-0.305	-0.364	-0.254	70
80	-0.106	-0.125	-0.091	-0.158	-0.168	-0.147	-0.208	-0.246	-0.191	80
90	-0.037	-0.043	-0.031	-0.066	-0.073	-0.100	-0.082	-0.082	-0.076	90
100	+0.097	+0.097	+0.097	+0.100	+0.099	+0.099	+0.100	+0.102	+0.102	100

TABLE V (Cont.)

Values of C_p

α	$M_o \approx 0.84$ 0°	$M_o \approx 0.84$ +1° Upper Surface	$M_o \approx 0.84$ +1° Lower Surface	$M_o \approx 0.86$ 0°	$M_o \approx 0.86$ +1° Upper Surface	$M_o \approx 0.86$ +1° Lower Surface	$M_o \approx 0.88$ 0°	$M_o \approx 0.88$ +1° Upper Surface	$M_o \approx 0.88$ +1° Lower Surface	α
100 x/c \ M_o	0.840	0.840	0.840	0.861	0.861	0.861	0.881	0.880	0.880	M_o / 100 x/c
00	+1.185	+1.185	+1.185	+1.196	+1.196	+1.196	+1.208	+1.207	+1.207	00
0.25	+0.948	+0.910	+0.974	+0.960	+0.925	+0.996	+0.976	+0.940	+1.007	0.25
01	+0.664	+0.618	+0.712	+0.677	+0.636	+0.726	+0.693	+0.647	+0.733	01
03	+0.357	+0.312	+0.409	+0.375	+0.333	+0.427	+0.391	+0.345	+0.435	03
05	+0.226	+0.179	+0.276	+0.241	+0.201	+0.293	+0.258	+0.213	+0.303	05
08	+0.096	+0.051	+0.147	+0.112	+0.070	+0.164	+0.129	+0.082	+0.172	08
13	-0.011	-0.055	+0.079	+0.003	-0.036	+0.053	+0.021	-0.024	+0.062	13
20	-0.134	-0.177	-0.085	-0.120	-0.159	-0.071	-0.101	-0.143	-0.060	20
30	-0.291	-0.334	-0.241	-0.278	-0.316	-0.228	-0.257	-0.297	-0.216	30
40	-0.393	-0.442	-0.336	-0.388	-0.429	-0.335	-0.371	-0.412	-0.326	40
50	-0.423	-0.480	-0.356	-0.431	-0.474	-0.372	-0.415	-0.460	-0.370	50
60	-0.395	-0.480	-0.331	-0.442	-0.490	-0.359	-0.436	-0.482	-0.386	60
70	-0.341	-0.418	-0.279	-0.404	-0.478	-0.305	-0.430	-0.480	-0.360	70
80	-0.249	-0.316	-0.202	-0.327	-0.419	-0.236	-0.388	-0.456	-0.296	80
90	-0.092	-0.073	-0.086	-0.177	-0.318	-0.117	-0.306	-0.378	-0.202	90
100	+0.103	+0.106	+0 106	+0.113	+0.124	+0.124	+0.134	-0.009	-0.009	100

TABLE V (Cont.)

Values of C_p

α	$M_o \approx 0.89$ 0°	$M_o \approx 0.89$ $+1^\circ$ Upper Surface	$M_o \approx 0.89$ $+1^\circ$ Lower Surface	$M_o \approx 0.90$ 0°	$M_o \approx 0.90$ $+1^\circ$ Upper Surface	$M_o \approx 0.90$ $+1^\circ$ Lower Surface	$M_o \approx 0.91$ 0°	$M_o \approx 0.91$ $+1^\circ$ Upper Surface	$M_o \approx 0.91$ $+1^\circ$ Lower Surface	α
$100\ x/c$ \ M_o	0.891	0.891	0.891	0.902	0.902	0.902	0.912	0.913	0.913	M_o / $100\ x/c$
00	+1.213	+1.211	+1.211	+1.217	+1.218	+1.218	+1.226	+1.223	+1.223	00
0.25	+0.981	+0.948	+1.013	+0.987	+0.956	+1.020	+1.001	+0.965	+1.027	0.25
01	+0.701	+0.649	+0.734	+0.710	+0.676	+0.757	+0.718	+0.679	+0.757	01
03	+0.401	+0.348	+0.435	+0.411	+0.378	+0.461	+0.422	+0.381	+0.463	03
05	+0.267	+0.216	+0.302	+0.279	+0.246	+0.329	+0.290	+0.251	+0.330	05
08	+0.139	+0.087	+0.173	+0.150	+0.116	+0.199	+0.161	+0.123	+0.203	08
13	+0.031	-0.020	+0.063	+0.043	+0.011	+0.089	+0.054	+0.018	+0.093	13
20	-0.091	-0.139	-0.060	-0.079	-0.110	-0.033	-0.068	-0.102	-0.029	20
30	-0.246	-0.317	-0.216	-0.234	-0.262	-0.189	-0.222	-0.253	-0.176	30
40	-0.360	-0.407	-0.328	-0.347	-0.377	-0.303	-0.335	-0.366	-0.297	40
50	-0.408	-0.458	-0.372	-0.398	-0.427	-0.349	-0.387	-0.418	-0.346	50
60	-0.429	-0.491	-0.392	-0.420	-0.452	-0.372	-0.411	-0.444	-0.369	60
70	-0.427	-0.481	-0.387	-0.423	-0.451	-0.372	-0.414	-0.446	-0.372	70
80	-0.404	-0.458	-0.351	-0.412	-0.443	-0.359	-0.409	-0.440	-0.365	80
90	-0.335	-0.391	-0.286	-0.363	-0.390	-0.315	-0.384	-0.406	-0.348	90
100	-0.079	-0.136	-0.136	-0.293	-0.312	-0.312	-0.316	-0.329	-0.329	100

WT.2078.C.P.367.K3 - Printed in Great Britain.

TABLE V (Cont.)

Values of C_p

α	$M_o \approx 0.925$: 0^o	$M_o \approx 0.925$: $+1^o$ Upper Surface	$M_o \approx 0.925$: $+1^o$ Lower Surface	$M_o \approx 0.94$: 0^o	$M_o \approx 0.94$: $+1^o$ Upper Surface	$M_o \approx 0.94$: $+1^o$ Lower Surface	α
$100\ x/c$ \ M_o	0.926	0.925	0.925	0.940	0.940	0.940	M_o / $100\ x/c$
00	+1.232	+1.231	+1.231	+1.239	+1.239	+1.239	00
0.25	+1.009	+0.972	+1.033	+1.014	+0.983	+1.044	0.25
01	+0.729	+0.689	+0.766	+0.743	+0.705	+0.780	01
03	+0.433	+0.395	+0.474	+0.451	+0.412	+0.490	03
05	+0.304	+0.264	+0.343	+0.323	+0.284	+0.361	05
08	+0.177	+0.138	+0.216	+0.196	+0.157	+0.234	08
13	+0.070	+0.033	+0.107	+0.089	+0.053	+0.127	13
20	-0.050	-0.085	-0.015	-0.030	-0.065	+0.006	20
30	-0.203	-0.237	-0.169	-0.181	-0.213	-0.146	30
40	-0.316	-0.350	-0.281	-0.294	-0.325	-0.259	40
50	-0.368	-0.402	-0.330	-0.327	-0.378	-0.309	50
60	-0.392	-0.429	-0.354	-0.372	-0.406	-0.333	60
70	-0.396	-0.431	-0.358	-0.377	-0.411	-0.338	70
80	-0.393	-0.427	-0.353	-0.374	-0.406	-0.336	80
90	-0.379	-0.408	-0.346	-0.365	-0.393	-0.330	90
100	-0.311	-0.327	-0.327	-0.300	-0.312	-0.312	100

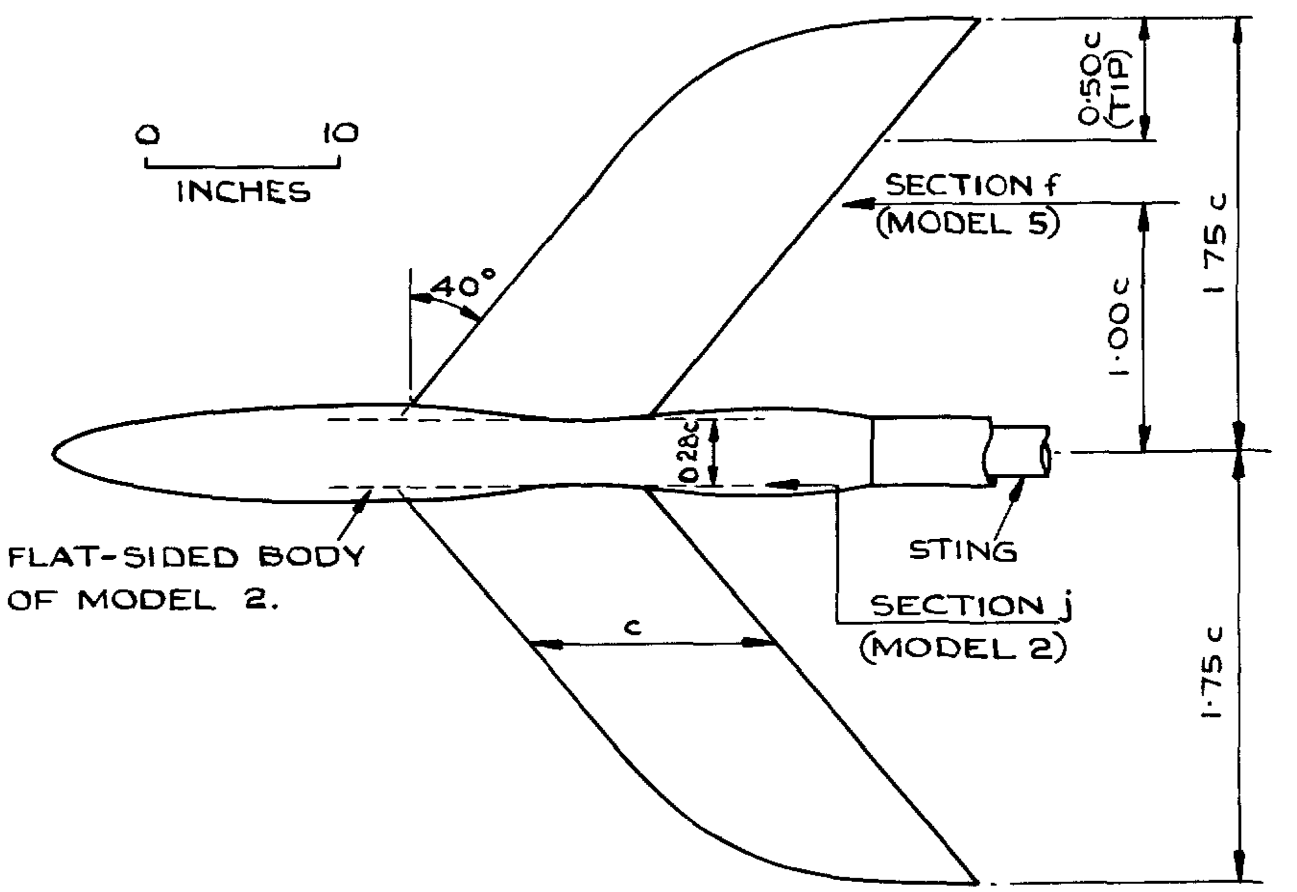

FIG. 1. MODEL 5 OF REFS. 1 & 2.

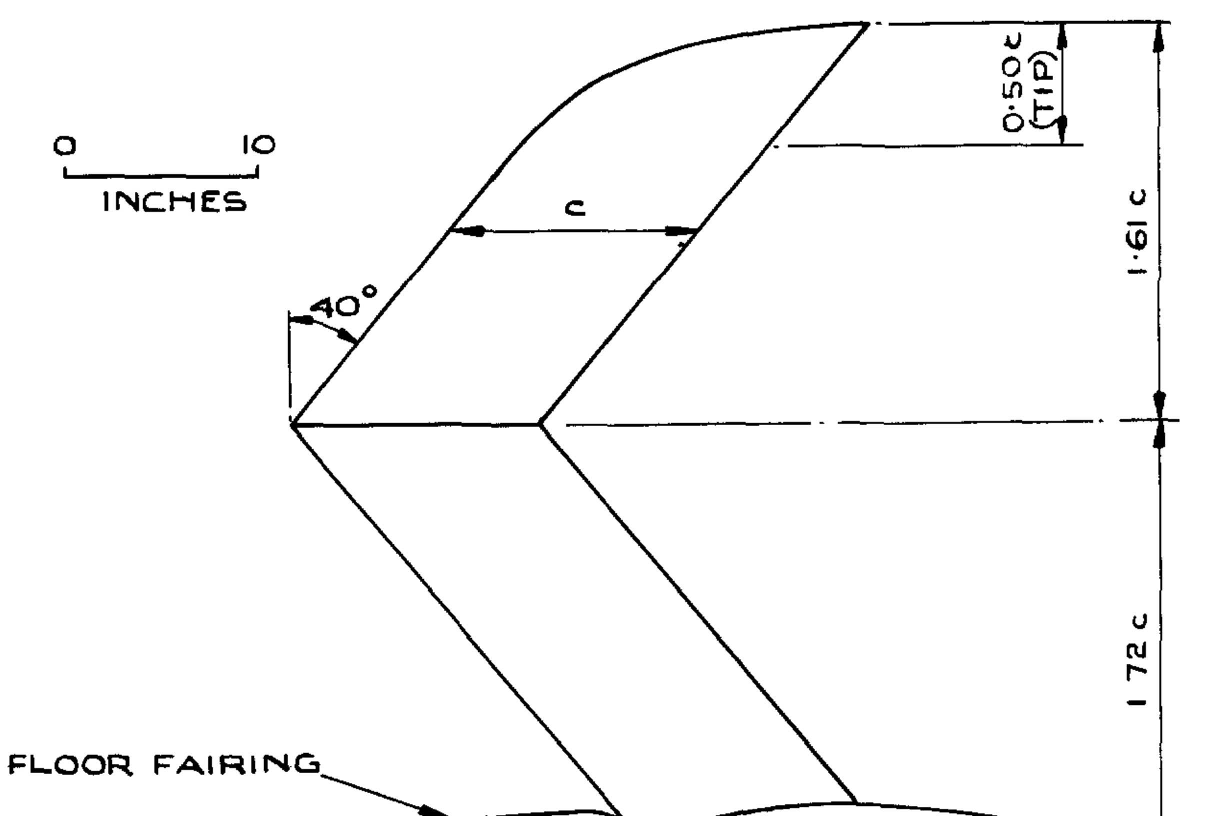

FIG. 2. WING AND FLOOR FAIRING OF PRESENT TESTS MOUNTED ON TUNNEL FLOOR.

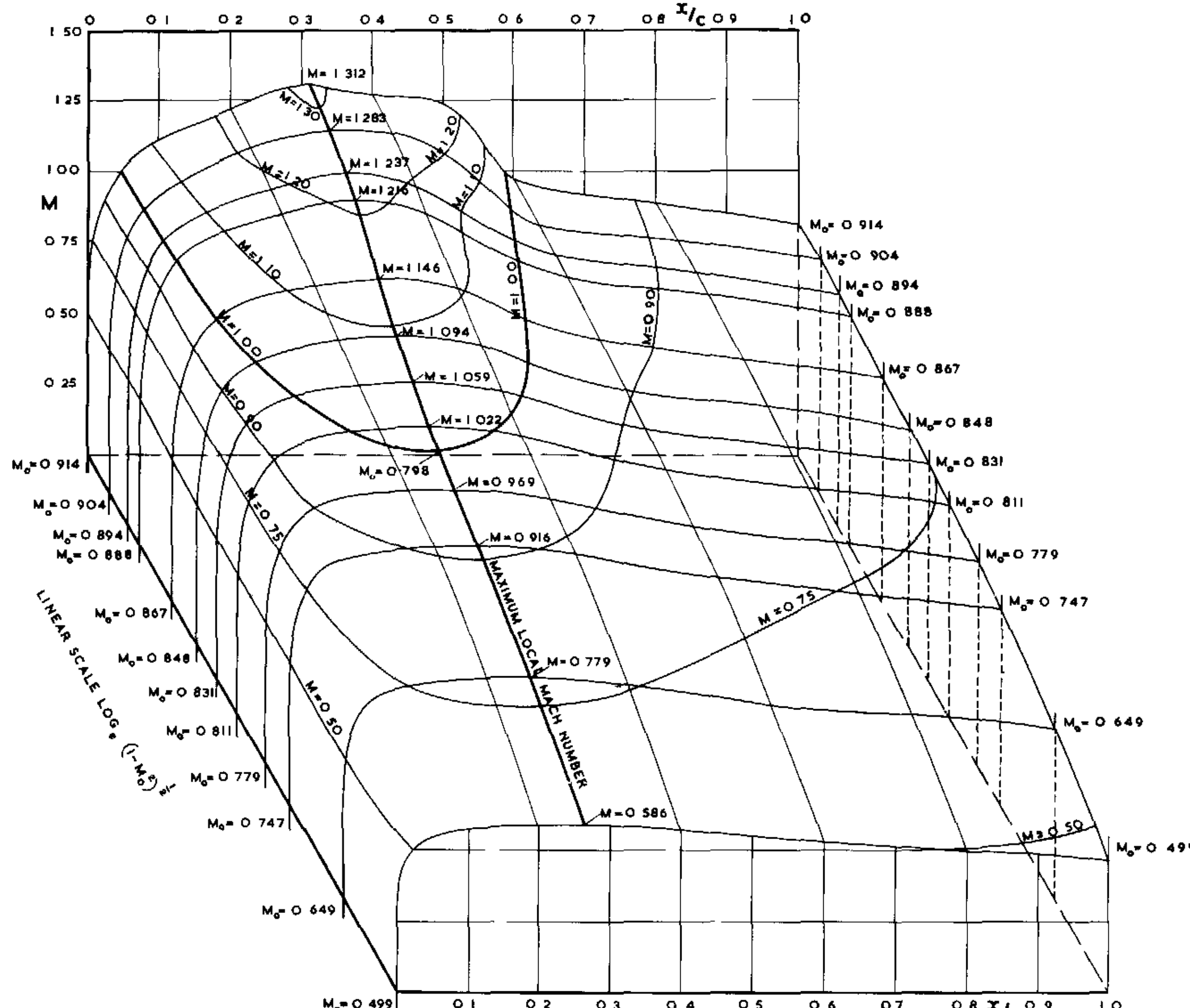

FIG 3 VARIATION OF LOCAL MACH Nº ALONG CHORD OF SHEARED WING AND WITH FREE-STREAM MACH Nº

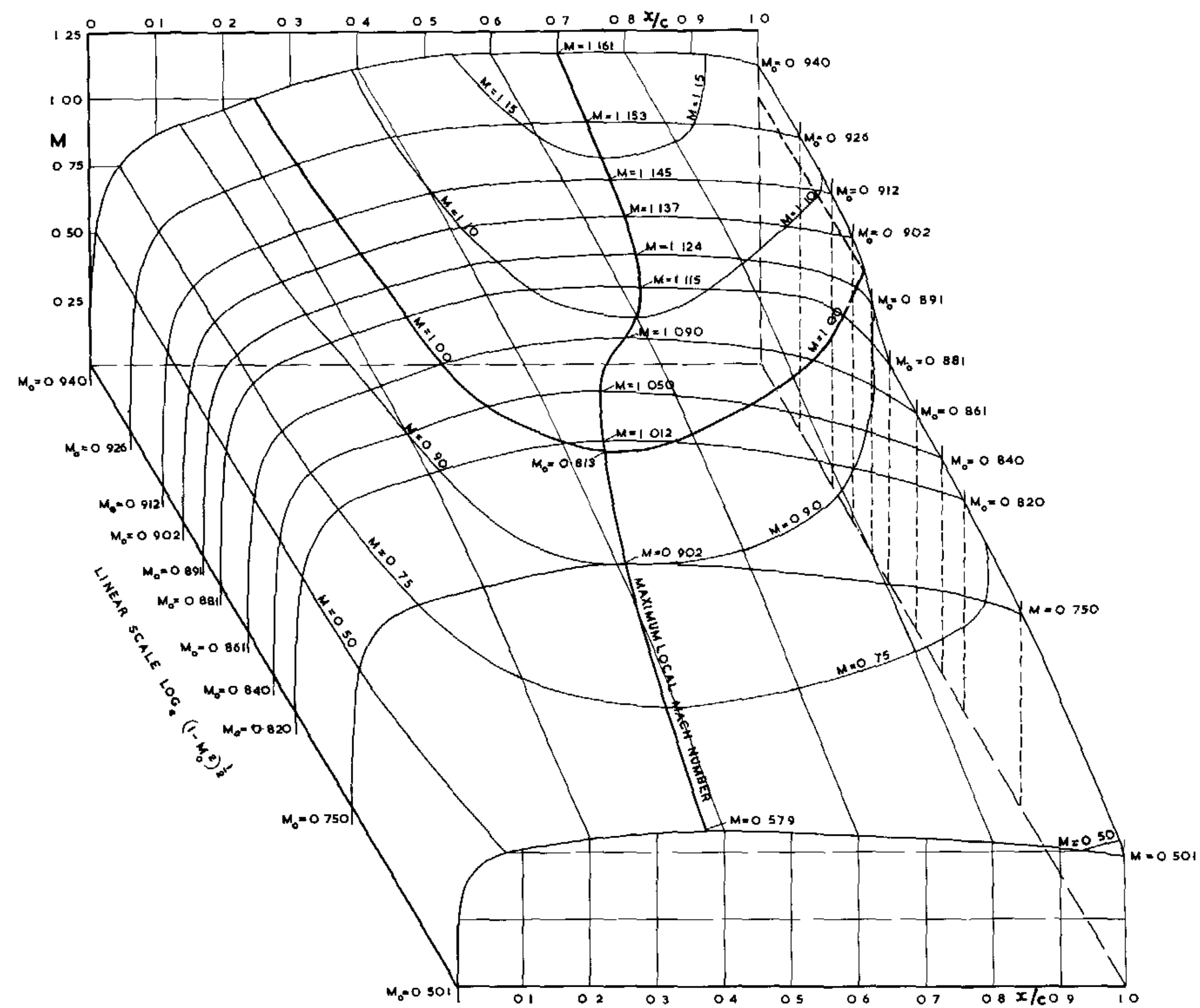

FIG 4 VARIATION OF LOCAL MACH Nº ALONG CHORD AT CENTRE SECTION AND WITH FREE-STREAM MACH Nº

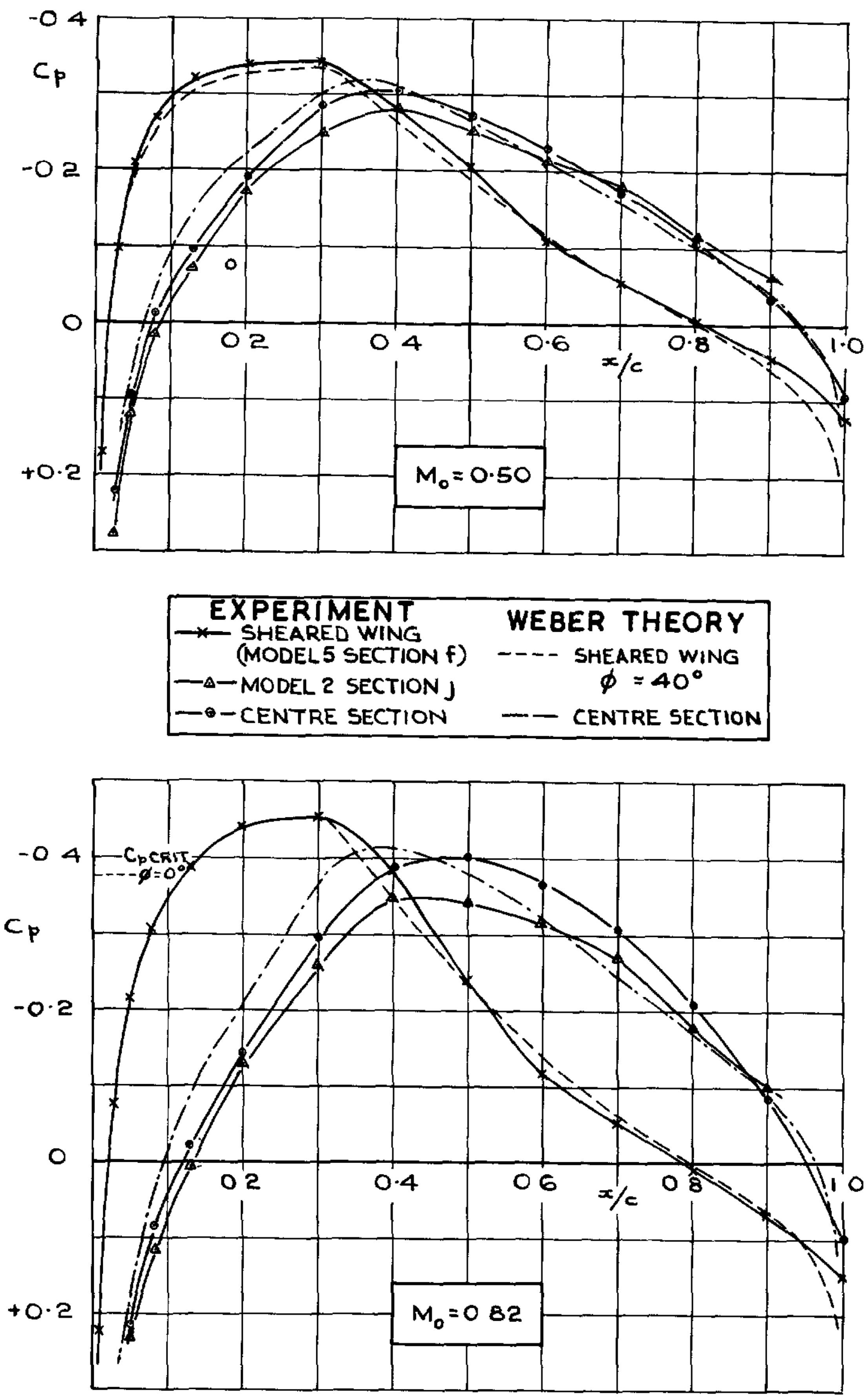

FIG. 5. (a) & (b) EXPERIMENTAL AND THEORETICAL PRESSURE DISTRIBTIONS ON A SWEPTBACK WING.

M = 0·50 & 0·82

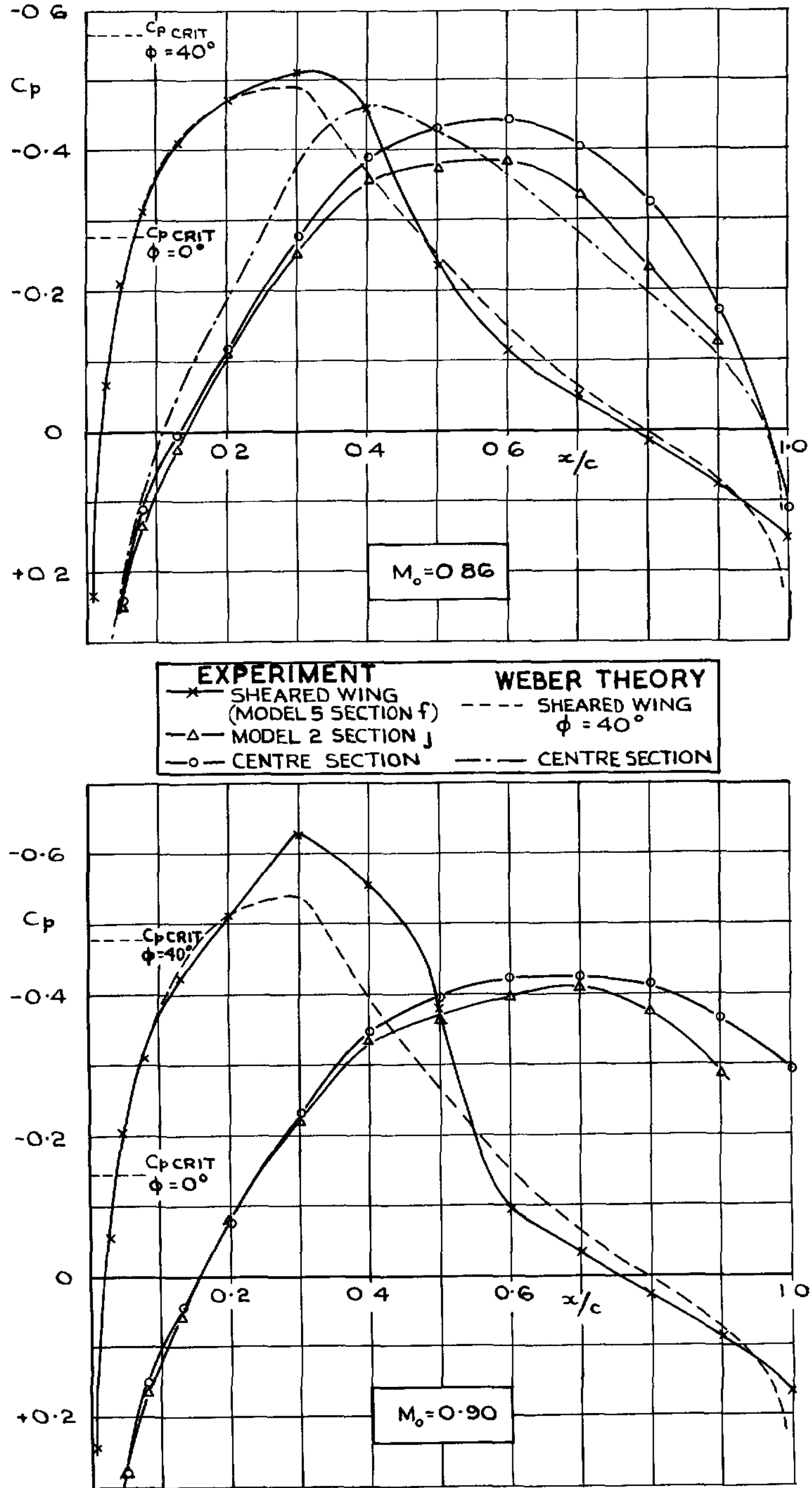

FIG. 5. (c) & (d) EXPERIMENTAL AND THEORETICAL PRESSURE DISTRIBUTIONS ON A SWEPTBACK WING.

$M_o = 0.86$ & 0.90

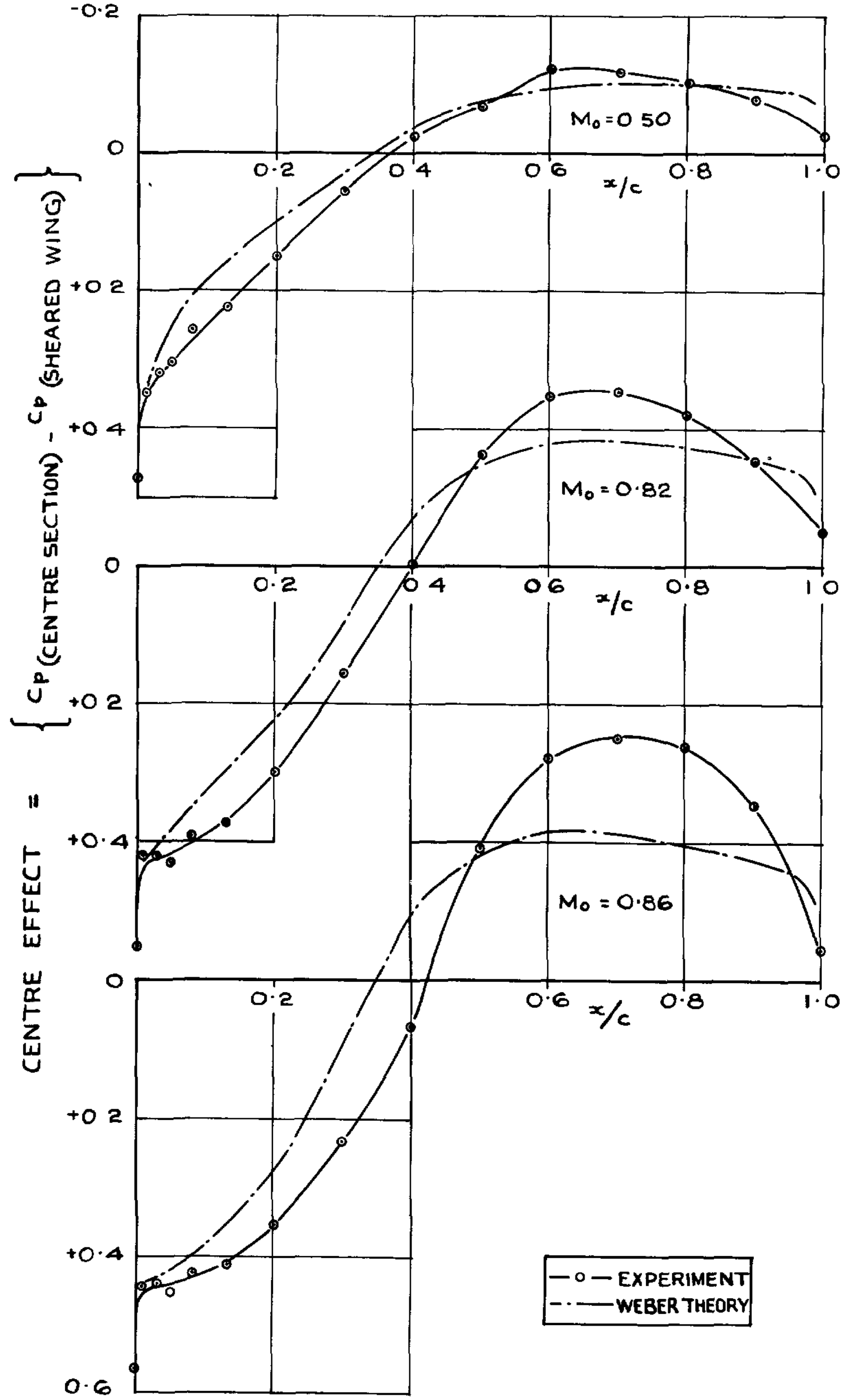

FIG 6. EXPERIMENTAL AND THEORETICAL CENTRE EFFECTS AT M_0 = 0·50 0·82 & 0·86.

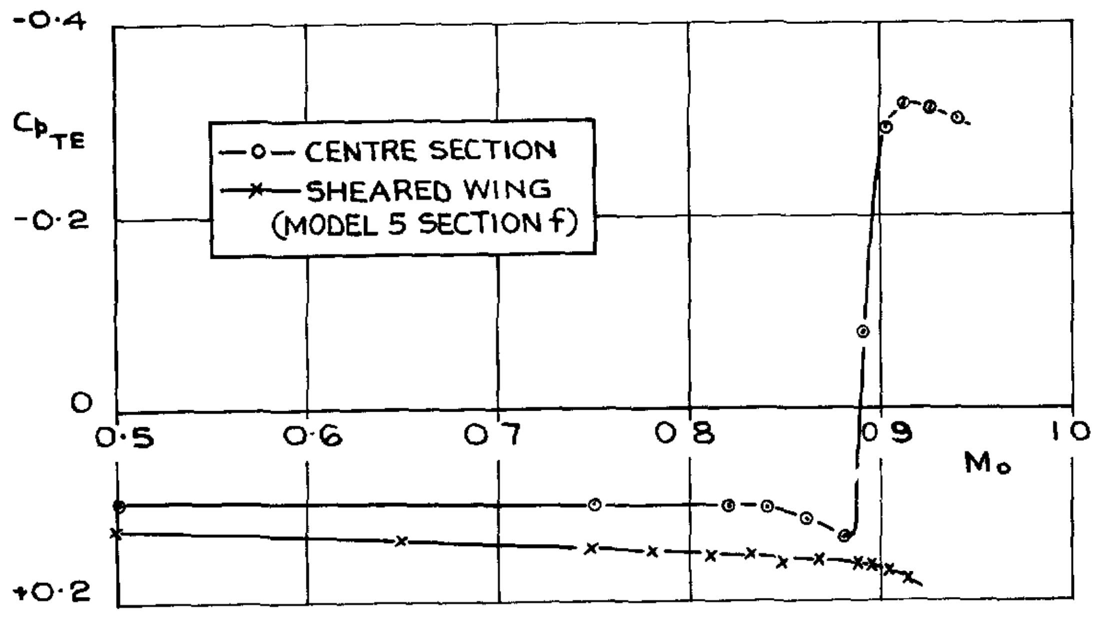

FIG 7. VARIATION OF TRAILING EDGE PRESSURE COEFFICIENT WITH FREE-STREAM MACH NUMBER

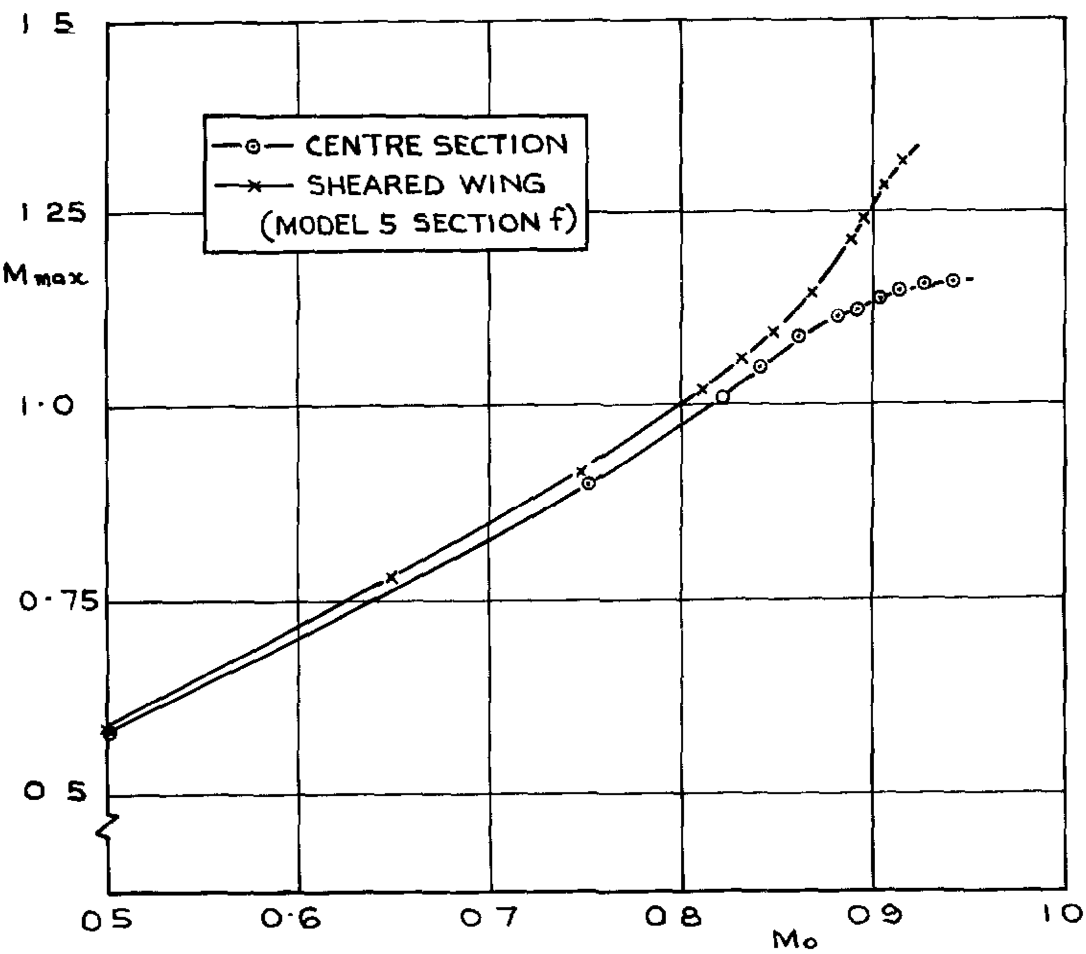

FIG. 8. VARIATION OF MAXIMUM LOCAL MACH. NUMBER WITH FREE-STREAM MACH NUMBER

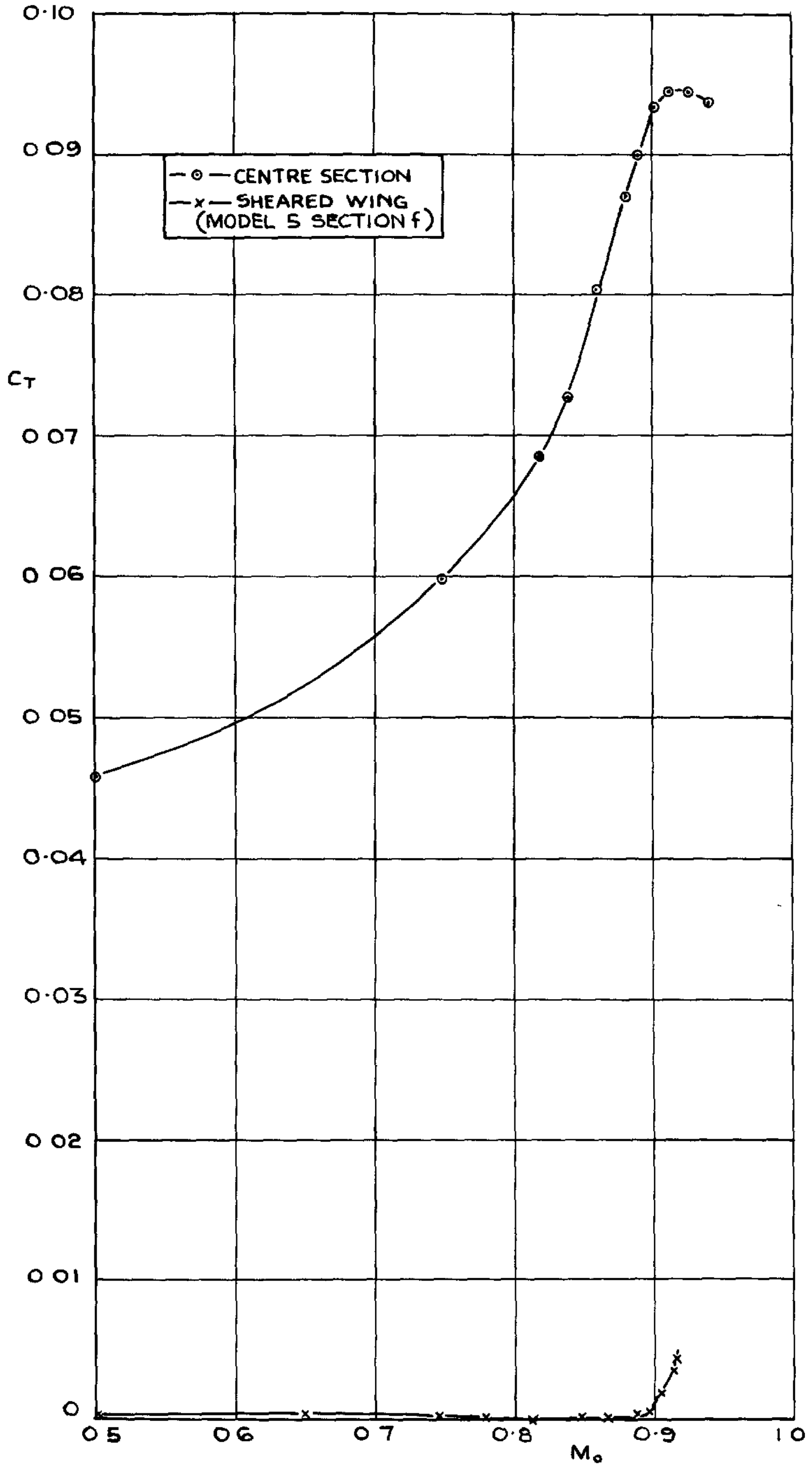

FIG. 9. VARIATION OF TANGENTIAL PRESSURE-FORCE COEFFICIENT WITH FREE-STREAM MACH NUMBER.

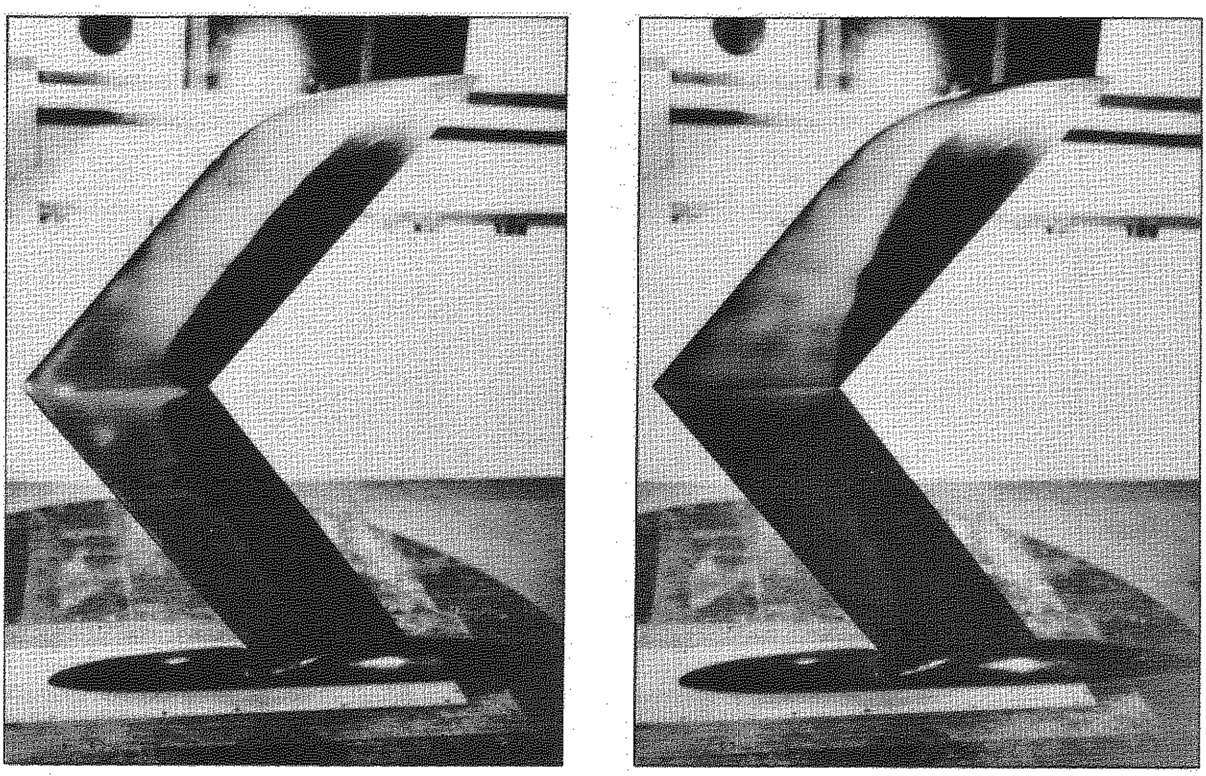

M = 0.50 M = 0.91

FIG.10. TRANSITION POSITIONS AT M_0 = 0.50 AND M_0 = 0.91

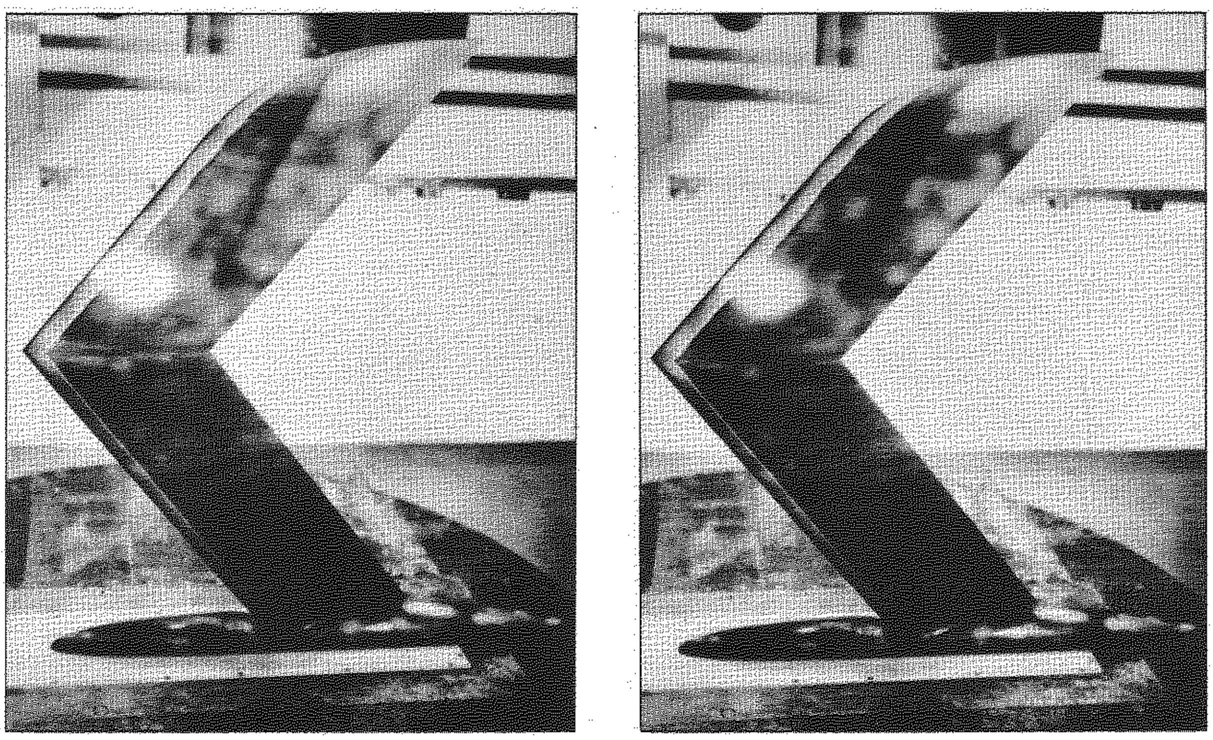

5 MINS. 6 MINS.

FIG11. SHOCK-WAVE POSITIONS AT M_0 = 0.91 AFTER
5 AND 6 MINUTES RUNNING TIME
(TRANSITION FIXED AT 10% CHORD)

C.P. No. 367
(18,998)
A.R.C. Technical Report

Published by
HER MAJESTY'S STATIONERY OFFICE

To be purchased from
York House, Kingsway, London W C 2
423 Oxford Street, London W 1
13A Castle Street, Edinburgh 2
109 St Mary Street, Cardiff
39 King Street, Manchester 2
Tower Lane, Bristol 1
2 Edmund Street, Birmingham 3
80 Chichester Street, Belfast
or through any bookseller

PRINTED IN GREAT BRITAIN

S.O. Code No. 23-9010-67

C.P. No. 367